Characterization of X-UV multilayers by grazing incidence X-ray reflectometry

L. Nevot, B. Pardo, J. Corno

Revue Phys. Appl. **23** (1988) 1675-1686 OCTOBRE **1988,** PAGE 1675

Classification
Physics Abstracts
68.55 — 68.60 — 78.65 — 42.80D — 61.10F — 06.30C — 07.60H

Characterization of X-UV multilayers by grazing incidence X-ray reflectometry

L. Nevot, B. Pardo and J. Corno

Institut d'Optique Théorique et Appliquée, Unité Associée 14 du CNRS, Bât. 503 Centre Universitaire, B.P. 43, 91406 Orsay Cedex, France

(*Reçu le 3 juillet 1987, révisé le 31 mai 1988, accepté le 2 juin 1988*)

Résumé. — Les performances des multicouches dans le domaine X-UV sont tributaires des défauts structurels et géométriques des matériaux déposés. Ces défauts sont difficiles à différencier par l'analyse d'un seul pic de Bragg tel qu'observé en X mous. Dès lors, la prédiction des performances pour d'autres longueurs d'onde, devient délicate. Nous montrons comment la réflectométrie de rayons X rasants (Cu $K\alpha_1$) permet de déterminer à la fois les rugosités interfaciales et les écarts d'épaisseur, ainsi que leur évolution au sein de l'empilement. Trois multicouches (W/C), de périodes comprises entre 3 et 6 nm et comportant de 20 à 40 couches élémentaires, sont analysées à titre d'exemples.

Abstract. — The performance of multilayers at the X-UV wavelengths depends upon the structural and geometrical imperfections of the deposited materials. These two respective contributions are not easily separated when only one Bragg peak is recorded, as is usually the case in the X-UV range, so a prediction of the performance at other wavelengths appears rather doubtful. We show how grazing incidence X-ray reflectometry (using Cu $K\alpha_1$ radiation) allows the precise evaluation of both interfacial roughnesses and thickness errors, as well as their variations through the stacks. As examples, we analyse three (W/C) multilayers with periods between 3 to 6 nm and up to 40 layers.

1. Introduction.

During the last ten years, there has been a considerable development of studies aiming at the preparation of stratified and periodic media having layer thicknesses on the order of only few nanometers. Such media indeed open many prospects in various fields, for example : superconductivity [1], magnetism [2], microelectronics [3], neutron optics [4] and X-UV optics [5]. In the last case, the stacks are made of alternating thin films of materials which are, succesively, absorbing then transparent for the considered radiations. They allow, in particular, to increase considerably the mirror reflectivity while selecting a given wavelength according to the incidence angle of the X-ray beam. Consequently, these stacks act as monochromators, obeying the Bragg law, and their periodicity can be easily adapted to a chosen wavelength, λ, over the entire X-UV range ($1 < \lambda < 30$ nm). It is worth recalling that, in this wavelength range, most natural crystals cannot be used because of a too small reticular spacing, and that Langmuir-Blodgett layers present a too short lifetime under usual synchrotron fluxes.

For a given wavelength and a given pair of materials (provided their dielectric constants ε are very close to 1), the dynamical theory of the X-ray diffraction allows one to predict the maximum attainable reflectivity, the number of bilayers and their optimum thickness ratio [6]. It can be shown that the maximum reflectivity R_{max} depends only on two parameters : X and Y, related to the real and imaginary parts of the dielectric constants of the absorbing (ε_L) and transparent (ε_1) media by :

$$X = \text{Im}\ (\varepsilon_1)/\text{Im}\ (\varepsilon_L)$$
$$Y = \text{Re}\ (\varepsilon_1 - \varepsilon_L)/\text{Im}\ (\varepsilon_1 - \varepsilon_L)\,.$$

The iso-reflectivity curves can be drawn as abacuses (see Fig. 1) for a rapid and easy determination of R_{max}. Now, the experimental reflectivities are most often lower, and even much lower, than the values predicted by the theory, whatever the materials in the multilayer and their deposition method : evaporation with an electron gun with *in-situ* control of the

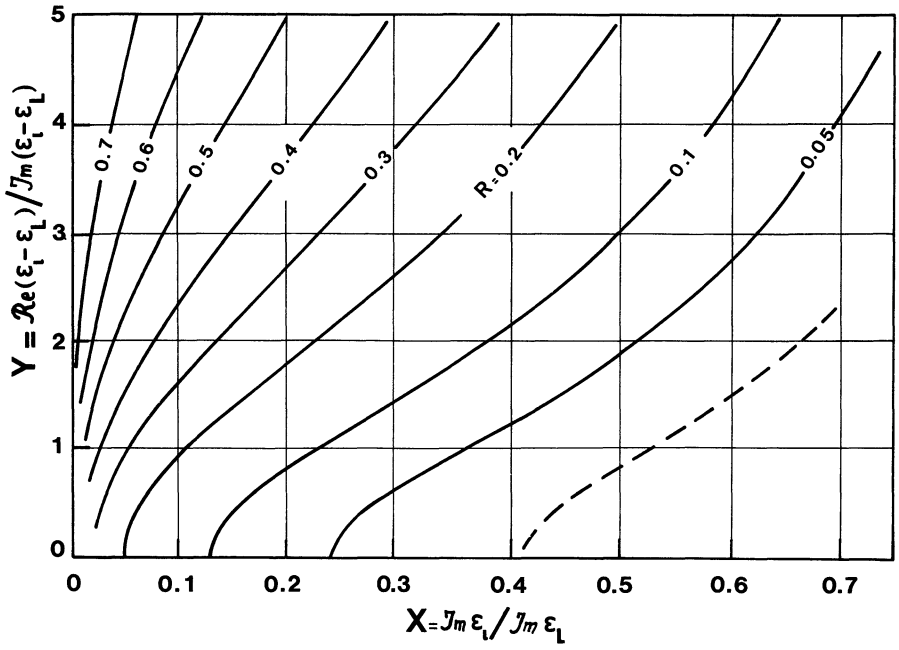

Fig. 1. — The calculated optimum specular reflectivity R, assuming perfect bi-layer stacks, is plotted *versus* two parameters which depend only on the dielectric constants of the absorbing or transparent media (ε_L, ε_l respectively). For a Ti/Ni multilayer, using the ε values published by Vinogradov and Zeldovich [6] at NKα wavelength (3.16 nm), we deduce $X = 0.27$, $Y = 3.79$ and $R_{max} = 32$ %. For a C/Cr multilayer, irradiated by BeKα radiation (11.4 nm), we obtain $X = 0.209$, $Y = 1.335$ and $R_{max} = 15$ %. Using the optical constants reported by Henke *et al.* [7], R_{max} becomes 35 % and 23 % respectively.

thickness by soft X-ray reflection [8], triode D.C. sputtering [9], magnetron diode D.C. sputtering [10-11], diode R.F. sputtering with ellipsometric control [12], or laser evaporation [13]. The only exception to that observation is a (Mo/Si) stack produced by Barbee *et al.* [14] and analysed under various radiations (16.01, 17.04 and 22.8 nm wavelengths).

Many factors modify the reflectivity from that computed within the assumption of strictly periodic stacks as well as of homogeneous and flat layers. For example, geometrical defects (deviations of the thicknesses with respect to their optimum values, variation of these thicknesses through the stack, interfacial roughnesses) and/or structural and compositional defects of the deposited materials themselves can be invoked. Besides, for instrumental reasons, absolute measurements of the reflectivity in the X-UV range prove to be rather difficult.

We intend to show how these different disorders in X-UV multilayers can be taken into account by the analysis of the X-ray reflectivity at grazing incidence (Cu Kα_1 radiation with 0.15405 nm wavelength). As examples, we will analyse three (W/C) stacks with periods between 3 and 6 nm, produced by diode sputtering.

2. Elements of theory and interface models.

2.1 HOMOGENEOUS AND PLANE MEDIA. — The reflectivity of an ideal multilayer (homogeneous media limited by sharp plane interfaces) can be computed either by the dynamical theory of X-ray diffraction or by the optical theory of stratified media. However it can be noticed that, for X-rays at grazing incidence, the apparent wavelength of the exciting radiation, i.e. $\lambda/\sin\theta$ (where λ represents the wavelength, of the order of 0.1 nm, and Θ is the grazing angle of the incident X-ray beam with respect to the average plane of the illuminated surface, of the order of 1 degree) is much larger than the interatomic distances in the considered materials. On the other hand, the extent of the Fresnel zones with equal phase, in the planes parallel to the surface, is considerable as compared to the size of the grains or microcrystals which can develop in metallic layers. The medium inside each layer parallel to the surface will therefore be considered as continuous, and only the variation of ε with the depth z will be taken into account. Moreover, if different materials or elements are present in the same layer at a depth z, this layer will be characterized by the average value of the dielectric constants of the different elements with their respective concentrations. This last remark will in particular be worked out when modelizing the interfaces of the real multilayers.

Each medium is then represented by its complex index of refraction, n, related to the dielectric constant by : $\varepsilon = n^2$, and commonly written, for the wavelength λ in the X-ray range, as :

$$n = 1 - \delta - i\beta = 1 - (r_e/2\pi)\lambda^2 \sum_i N_i \tilde{f}_i$$

where r_e stands for the classical electron radius, N_i for the number of atoms per unit volume for the atomic species i, $\tilde{f}_i$ for the atomic scattering factor. In the classical X-ray range ($\lambda \sim 0.1$ nm), $R_e \tilde{f}_i(0)$ is practically equivalent to Z_i, the atomic number of the considered element ; the anomalous dispersion correction remains indeed very small, and does not exceed $(Z_i/10)$ in most cases [16]. The values calculated by Cromer and Liberman are often used as reference, although the relativistic correction seems to be overestimated [17]. The δ values can be considered as being known to better than 1 % for classical X-rays, which is a much better accuracy than in the X-UV range. On the other hand, it is worth remembering that here δ reflects essentially the electronic density of the medium. β is directly deduced from the linear absorption coefficient μ of the material (16b) through the relation : $\beta = \mu\lambda/4\pi$.

The theoretical δ and β values for the (W/C) pair and Cu $K\alpha_1$ radiation are reported in table I.

Table I. — *Theoretical values of the optical indices* (δ, β) *for carbon and tungsten irradiated with* Cu$K\alpha_1$ X-*rays.*

Material	Density	δ ($\times 10^{-6}$)	β ($\times 10^{-6}$)
C	2.05	6.6	0.01
W	19.30	45.74	4.03

The specular reflectivity of a stack of ideal layers can easily be computed with the optical theory of stratified media [18]. The boundary conditions, which imply the continuity of the tangential components of the electric and magnetic fields, allow one to obtain various recurrent formulations using, either the matrix calculus, or the impedance notion. We also quote the Parratt method [19], developed by Underwood and Barbee [20]. The reflection and transmission coefficients for a single plane boundary between two homogeneous media are obtained with the help of the Fresnel solutions. It should be noticed that, for grazing incidence X-rays, the specular reflectivity is the same whatever the polarization of the incident wave. This results in a simplification, both instrumental for the absolute reflectivity measurements, and theoretical for the interpretation of these measurements.

2.2 ROUGH AND (OR) INHOMOGENEOUS INTERFACES. — In practice, the interfaces between the various layers are neither sharp nor flat. Not only the existence of roughnesses, but also composition modifications related for example to different diffusion processes, must be taken into consideration. In some cases, such effects are even desirable and are generated either by thermal treatments or by ionic irradiation.

We have already stated that, for grazing incidence X-rays, the interfacial region appears like a transition layer in which the refractive index varies continuously with the depth z. The interface is then divided into elementary layers where the index $n(z)$ will depend on the roughnesses distribution and/or on the possible diffusion mechanisms.

For a rough interface between two homogeneous materials with indices n_1 and n_2, where the height of the surface is randomly distributed (see Fig. 2), $n(z)$ may be represented by an Error function :

$$n(z) = n_1 + (n_2 - n_1)\,\mathrm{Erf}\,(z, \sigma)$$

with

$$\mathrm{Erf}\,(z, \sigma) = (\sigma\sqrt{2\pi})^{-1} \int_{-\infty}^{z} \exp(-\xi^2/2\sigma^2)\,d\xi\,.$$

The surface roughness will be defined by σ, the standard deviation of the Gaussian distribution, or

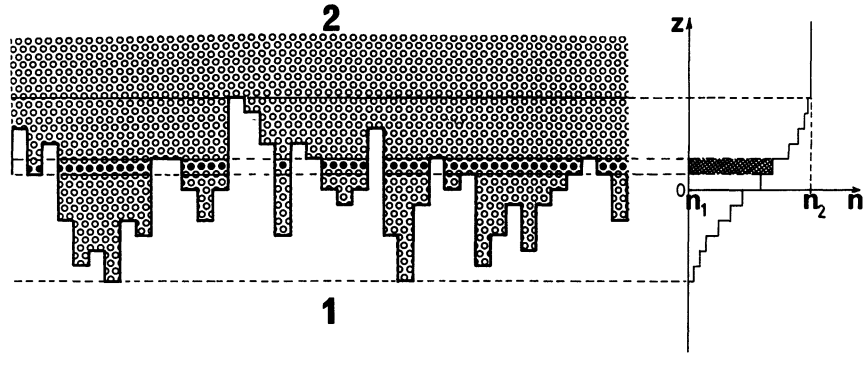

Fig. 2. — Schematic drawing of the rough boundary between two homogeneous materials with refractive indices n_1, n_2. If the roughnesses are randomly distributed, the refractive index profile $n(z)$ along the z axis, normal to the surface, is an error-function through the transition layer, as plotted as a histogram on the right of the figure.

the root-mean-square value of the height with respect to the average plane of the interface [21]. Other $n(z)$ laws have also been used, for example, the linear law [22] and the sinusoïdal law [20].

This method of the transition layer offers the possibility to be easily generalized to any real type of diffuse interface, but it presents a major disadvantage in the case of multilayers requiring large computation times which become rapidly prohibitive.

Mathematical equivalences can be obtained for random rough interfaces [23]. If the roughness spectrum exhibits a preponderance of the high spatial frequencies (typically $\nu_s > 1\ \mu m^{-1}$) [24], the specular reflectivity $R(\Theta)$ of the rough boundary will simply be deduced from that of the smooth and flat boundary $R_0(\Theta)$ by the relation :

$$R(\Theta) = R_0(\Theta) \exp(-16\ \pi^2 K_{1n} K_{2n} \sigma^2) \quad (2.1)$$

in which K_{1n} and K_{2n} refer to the normal components of the wave vectors in the two media ($\|K\| = 1/\lambda$).

In the opposite case (preponderance of the low spatial frequencies), the relation is :

$$R(\Theta) = R_0(\Theta) \exp(-16\ \pi^2 K_{1n}^2 \sigma^2) . \quad (2.2)$$

It must be noticed that these two damping terms are only equivalent to the well-known Debye-Waller term, $\exp(-16\ \pi^2 \sigma^2 \sin^2 \Theta/\lambda^2)$, far from the total reflection limit (which is defined by $\Theta_c \approx \sqrt{2\ \delta}$). On the other hand, they are strongly different in the vicinity of Θ_c (see Fig. 3 in [23]). Only the « high frequencies » damping term allows one to obtain values close to the ones computed with the error function transition layer, provided σ is not too high ($\sigma \leqslant 1.5$ nm).

The extension to the case of a multilayer with rough interfaces is easily obtained by modifying, in the Fresnel solutions, the reflection amplitude coefficients by the term $\exp(-8\ \pi^2 K_{1n} K_{2n} \sigma^2)$ corresponding to each interface. As for the transmission coefficients, two situations can be considered [25] :

(i) either the rough interface does not introduce any global energy loss by scattering ; in this case the transmission coefficient is increased in order to compensate for the attenuation produced on the reflection.

(ii) or, there is a global energy loss coming only from the reflection : the transmission coefficient remains unchanged.

The first assumption is usually the one which is retained, because the roughnesses of the thin films which are presently deposited are small enough.

In other respects, it has often been admitted up to now [26, 27] that the interfaces of very thin films were identical, or became so when a sufficient number of periods are deposited. Under the assumption of identical rough interfaces, the expressions (2.1) and (2.2) can be directly used in order to deduce the specular reflectivity of the multilayer, $R_0(\Theta)$ being then associated with the ideal multilayer. This situation appears somewhat exceptional.

The analyses made on the X-ray scattering according to the grating law [28] allow, in the case of homogeneous, metallic or dielectric thin films with thicknesses of a few 10 nm, to determine both the roughnesses of the limiting surfaces and the interprofile correlation. The conclusion is that, not only are the roughnesses of the substrate interface and of the free surface usually different, but also the interprofile correlation tends to disappear towards the high spatial frequencies. The assumption of identical multilayers must not constitute a systematic pre-requisite for the analysis of their reflectivity, a same « mean effective » roughness given by the only multiplicative Debye-Waller factor being able of account for very different roughness changes.

Moreover, the value found after analysis of the reflectivity at the Bragg maxima under Cu $K\alpha_1$ radiation is not always confirmed by the one obtained with soft X-rays [12, 13].

Another discrimination parameter, at least qualitatively, could be given by the width at half-height $\Delta\Theta_B$ of the Bragg peaks [29]. A degradation of the interfacial roughness implies an increase of $\Delta\Theta_B$. For identical multilayers $\Delta\Theta_B$ remains approximately the same as for the ideal multilayer.

2.3 THICKNESS ERRORS IN THE STACK. — Thickness errors can be made during the film deposition. For example in cathodic sputtering systems, some parameters which define the plasma and/or the deposition rate (gaz pressure, target voltage, substrate temperature) are liable to shift or to fluctuate.

In the methods using an *in-situ* thickness control, checking errors cannot be avoided, even if the principle of these methods allows one to compensate for the error made on the preceding deposited film. These errors affect not only the shape and the intensity of the Bragg peaks, but also the angular positions and the contrasts of the secondary maxima [29]. When the number of layers in the stack is too high for the secondary maxima to be resolved by the reflectometer, it can become difficult to discriminate between the roughness and the thickness error effects.

In the case of random errors on the thicknesses, Spiller and Rosenbluth [30] have developed a model that gets rid of the roughnesses. The variance of these errors can be obtained from the comparison of the intensities of the continuous backgrounds for the Bragg half-orders in between the main peaks and that of the latter. It must however be underlined that this model can only be applied if the roughnesses are identical for all the layers. Besides, the absolute

measurement of very small fluxes, close to the background noise of the experimental set-up, is very delicate.

3. Experimental set-up.

The principle of an X-ray reflectometry set-up has already been described by Parratt [19]. The performances of the present reflectometers are due to the technological improvements achieved since then, in both electronics and mechanics. Since the material index of refraction is smaller than 1, there is an angular region of « total » reflection, the limite θ_c of which is easily deduced from δ by the Snell-Descartes relations, i.e. $\theta_c = \sqrt{2(\delta^2 + \beta^2)^{1/2}}$ or $\theta_c \approx \sqrt{2\,\delta}$ if absorption is negligible ($\beta \ll \delta$). With $\lambda \sim 0.1$ nm and $\delta \approx 10^{-5}$, θ_c is of the order of 3 mrad. Beyond, the specular reflectivity R decreases rapidly ; the $R(\theta)$ data therefore concern only very grazing angles (typically from 0 to 5 degrees).

The reflectometer built at the Institut d'Optique has source and detector arms 51.25 cm long, the angular mechanical accuracy is 1 second of arc. The arm rotations are accomplished with stepping motors (Microcontrole UE7PP). The X-ray source is a sealed tube with a copper anticathode (Tubix) with a linear focus (0.1×10 mm) supplied under 40 KV and 10 mA with a Philips PW 1011 generator. The cooling water is regulated both in flow and temperature (F. R. Cooling SCU 3). The $K\alpha_1\, K\alpha_2$ doublet is selected with the help of a plane quartz $(10\bar{1}1)$ monochromator. The $K\alpha_2$ radiation is then eliminated with a variable width slit (60 μm in most cases) located at 35 cm from the monochromator.

We recall that the reflectometer built by Segmuller [31] uses a two crystal Ge (220) monochromator, the intrinsic angular divergence of the X-ray beam being 5.9×10^{-2} mrad. The four crystal Ge (220) monochromator advocated by Bartels [32] allows one to take advantage of the (440) reflection without modifying the beam alignment, and the angular divergence is lowered by a factor of 2, but at the expense of an appreciable decrease of the X-ray intensity. This set-up with a point X-ray source seems mainly devised for the analyses on the semiconductor superlattices.

The sample to be analyzed is maintained on the object-holder stage by depression. The surface alignment is achieved using a retractable knife edge or a pre-adjusted telescopic sight.

During the analysis, the illuminated area varies as $(1/\sin\theta)$. In the vicinity of θ_c, it is frequently of the order of 1 cm^2. It is important to control the surface flatness in order to avoid geometrical effects which can perturb the $R(\theta)$ measurements. A float-glass substrate which is thick enough (at least 6 mm) often offers a good flatness and a small roughness ($\sigma \approx 0.4$ nm). On the other hand, the very thin silicon wafers (a few 0.1 mm thick) show facets and figure deviations which can modify strongly the absolute $R(\theta)$ measurements. In some cases, we were led to compensate for these deviations by using an object-holder with mechanical deformation (obtained with a set of screws) while controlling with visible light, the interference colours generated by the air gap between the silicon surface and the reference optical surface [33]. The direct analysis of the grazing X-ray specular reflection obtained on these silicon (111) wafers is usually performed by assuming the existence of a SiO_x ($1 < x < 2$) layer, about 2 nm thick, the free surface roughness being of 0.75 nm and the inner interface one of 0.28 nm.

The detection of the reflected X photons is performed with the help of a proportional counter (Xe/CH_4). A turret equipped with calibrated attenuation screens allows to keep a counting rate smaller than 10^3 counts per second. The slit located in front of the counter has a variable width from 10 to 200 μm, which allows one to choose either the angular resolution, or the number of photons detected for high grazing angles (11).

The entire instrumental set-up is driven by a personal computer (HP 85).

4. Experimental results.

4.1 EXAMPLE OF REGULAR MULTILAYER. — The $R(\theta)$ curve presented in figure 3 is that of a (W/C) stack deposited on a silicon substrate by Barbee. This stack is composed of 23 alternated layers, beginning and ending by a carbon layer. The experimental values are indicated by dots.

One clearly observes, between the 3 recorded Bragg peaks, the 9 secondary peaks expected in the case of 11 dense layers. The presence of these regularly distributed and well contrasted peaks demonstrates the very high reproducibility obtained during the deposition.

The theoretical curve (continuous line) has been calculated using the parameter values reported in table II for the elementary layers C, W and for the silicon substrate.

It must be noticed that the experimental values have been corrected for the background noise (0.1 count/second in this experiment) and normalized to the reflectivity measured in the total reflection region, and not to the intensity of the direct beam. This procedure is correct [33] when the examined surface presents a slight concavity (or convexity), and allows one to compensate for the convergence (or divergence) effects generated by the optical figure.

The optimization of the various parameters during the fit to the $R(\theta)$ experimental curves was more easily obtained by the selectivity of their influence in some part or other of the angular range as well as by

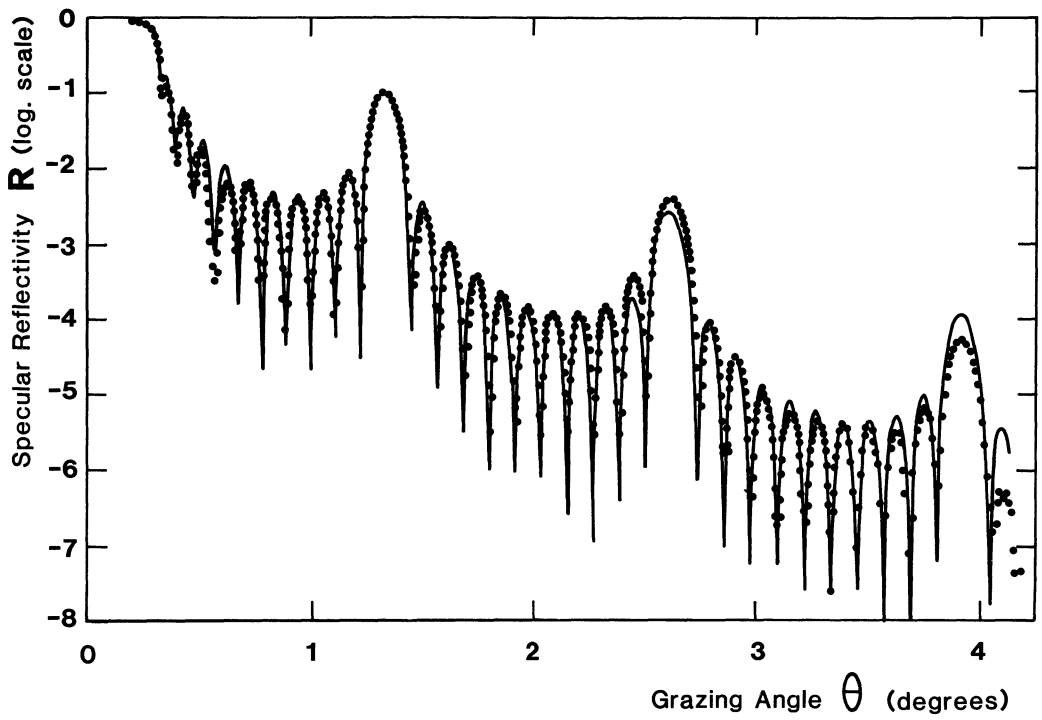

Fig. 3. — Measured (dots) and calculated (solid line) specular reflectivity $R(\theta)$ *versus* the grazing angle obtained with CuKα_1 radiation for a W/C stack containing 23 layers deposited onto a silicon substrate by magnetron sputtering (T. W. Barbee). The values of the fitting parameters are reported table II. The multilayer period is 3.375 nm.

the observation of many peaks. The average periodicity can be deduced from the angular position θ_k of the main Bragg peaks with the help of the Bragg law, after correction for the mean dispersion. The absorption correction is completely negligible in our case. It is however recalled that the general law is expressed by :

$$2\,d_c[\sin^2\theta_k - |1 - n_c^2|]^{1/2} + 2\,d_w[\sin^2\theta_k - |1 - n_w^2|]^{1/2} = k\lambda \quad (4.1)$$

where d_c and d_w are the thicknesses of the elementary layers, and k is the order of interference. For high enough grazing angles ($\theta \gg \theta_c$), this expression reduces to the classical law :

$$2(d_c + d_w)\sin\theta_k = k\lambda\ .$$

The period in the stack is thus determined independently of the true composition of the deposited materials.

The total reflection limit, which is determined by the first inflection point on $R(\theta)$, allows to determine the $\langle\delta\rangle$ value, and therefore the mean thicknesses of the layers of each material, in the case of multilayers having very thin dense layers. $\langle\delta\rangle$ is

Table II. — *Thicknesses, roughnesses and optical indices used for the* C/W *layers and* Si *substrate in order to obtain a good agreement with the experimental reflectivity curve shown figure* 3.

Material \ Parameter		Thickness	Roughness	Refractive index		Density
		nm	nm (r.m.s.)	δ ($\times 10^{-6}$)	β ($\times 10^{-6}$)	
Layers	C	2.575	0.325	6.6	0.01	2.05
	W	0.8	0.8	45.75	4.0	19.3
Substrate	SiO_x	2	0.75	5.25	0.08	1.6
	Si	∞	0.28	7.56	0.17	2.33

define as $(\Sigma_i d_i \delta_i / \Sigma_i d_i)$, i being the index of the considered layer. The material indices must be in agreement with the known bulk values or determined by a previous characterization of a single thin film with a thickness of at least 10 nm. Possible modifications of the compactness and/or composition of the materials as a function of the deposition parameters in a sputtering system can be detected in this way [34]. The existence of argon inclusions can be directly confirmed by a Rutherford backscattering analysis (11).

If the dense layers are a few nm thick, the summation concerns only a few layers which are the closest to the free surface. The evanescent waves generated for grazing angle smaller than or close to the critical angle of the absorbing material, practically vanish in the second dense layer. The extinction depth (defined at e^{-1} for the energy flow) written as [7, 19] : $\lambda / 4 \pi \sqrt{2 \delta}$ for $\theta = 0$ or $\lambda / 4 \pi \sqrt{\beta}$ for θ_c, is between 1.3 nm and 6.1 nm for pure tungsten with the CuKα_1 radiation.

A direct signature of the thicknesses is obtained when the thicknesses of the two elementary layers are in a simple ratio (for example 2, 3...). One then observes the disappearence or strong attenuation of the Bragg peaks of orders multiple of 3, 4... respectively. This is often seen on the $R(\theta)$ curve of stacks produced with *in situ* control by X-ray reflectivity. It must however be noticed that what is determined is the optical thicknesses of the layers, and that the refraction corrections are not negligible with soft X-rays. The ratio of the geometrical thicknesses can thus be modified [35].

The maxium intensities of the Bragg peaks are strongly correlated with the index difference integrated over a period and with the mean values of the W/C and C/W interfacial roughnesses. For convenience, the interfacial roughnesses $\sigma_{w/c}$ and $\sigma_{c/w}$ will be called σ_c and σ_w respectively, the C and W materials being looked at from the substrate to the free surface as during the deposition. If no perturbating process modifies the surface state of the previously deposited layer during the deposition of the subsequent layer, the interfacial roughness ($\sigma_{w/c}$, for example) in the stack is obviously identical to that of the initial surface (carbon, in the considered case). At last, the decrease of the mean reflected intensity just beyond θ_c depends essentially on the characteristics (index, thickness and roughness) of the last layer at the free surface.

The significant point of the analysis presented here concerns the clear difference between the W/C and C/W interfacial roughnesses. The σ_w roughness is of the same order as the thickness of the W elementary layer. The $\delta(z)$ profile shown in figure 4, over any period of the stack, expresses very well the greater scatter of the W atoms on the outer side than on the inner side. For comparison, we have drawn

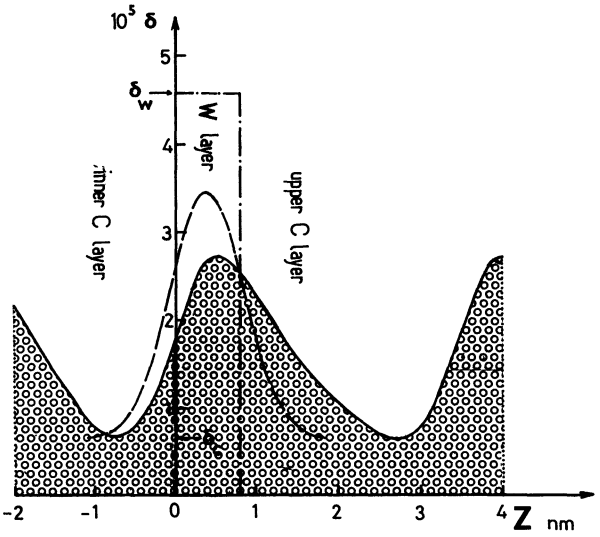

Fig. 4. — δ profile, normal to the surface, through any W layer in the stack. The origin of the z axis is at the W/C interface mean level. The rectangular profile (dot-dashed line) belong to an ideal W layer (flat boundaries). The dashed curve is for a layer having identical interfacial roughnesses ($\sigma_{W/C} = \sigma_{C/W} = 0.325$ nm). The full curve takes into account the fit roughness values of $\sigma_{W/C} = 0.325$ nm and $\sigma_{C/W} = 0.8$ nm.

the profiles associated with an identical W layer, i.e. with the same roughness σ_w and σ_c equal to 0.325 nm (dashed profile), and with an ideal W layer (rectangular profile). This elementary W layer, with an average thickness of 0.8 nm, can be viewed as islands which did not completely coalesce. The following C layer is thick enough to overlay these islands and to restore a smooth surface.

This interpretation can be compared to the results of electrical resistivity measurements [36] performed during the deposition of tungsten on a carbon layer with an electron gun under ultra-high vacuum. These measurements indicate that it is necessary to deposit at least 2 nm of W in order to obtain a continuous layer from an electrical point of view. For a deposit on a glass surface, 3 to 4 nm would be necessary. Also, the analysis of the soft X-ray reflectivity measured *in situ* in the same ultra-high vacuum equipment as before (37) reveal that the minimum roughness of the tungsten surface (about 0.2 nm) is reached for an average thickness of 4 to 5 nm (still on float-glass).

Although the values of the average thickness necessary to obtain a complete coalescence and a smooth surface can strongly depend on the deposition conditions and on the employed technique, it appears difficult to prepare a uniform tungsten layer for thicknesses smaller than 1 nm. Therefore, in order to optimize the performances of a multilayer for wavelengths of a few nanometers, it can prove more fruitful to try to produce, not the optimum

thickness values as given by the theory (on the basis of ideal thin films), but rather a thickness leading to a minimum surface roughness. In the same idea, it must not be forgotten that the roughness values which are determined by the grazing X-ray analysis represent the average contribution of the surface defects and ruggedness with a spatial period comprised between 10 nm and a few μm.

The observation of transverse cuttings of the stacks after ionic thinning by transmission electron microscopy allows a direct visualization of the interfacial regions over dimensions of a few tens of nm. Contrary to the analysis evoked before, the electron micrographs seem to indicate a much better regularity of the layer thicknesses, as well as nearly sharp interfaces [12, 38]. However, samples cut off in different places of the multilayer yield different relative thicknesses, even if the period value does not change [38]. When the analysis is made on a too large number of layers, artifacts linked to a very slight modification of the inclination of the layer planes with respect to the electron beam, can lead to a wrong interpretation of the progressive changes of the thicknesses during the stack fabrication [39]. In the case of a (W/Si) stack with a nominal period of 2.5 (including 0.5 nm of tungsten) produced by magnetron sputtering (Barbee), Petford-Long *et al.* [39] do not observe any real tungsten layer, but rather they see an amorphous interfacial region with mixed composition over a thickness of 1.3 nm. The silicon layers are amorphous too, and the Si/W interface is a little more diffuse than the W/Si interface. The opposite situation is found for a (W/C) multilayer produced by Energy Conversion Devices, with larger nominal thicknesses (2.4 nm for W and 3.6 nm for C). Tungsten appears as microcrystals. The presence of tungsten carbide WC is detected in the W/C interface, which is more extended than the C/W interface.

It is worth noticing that the introduction of an intermediate carbide phase over about 1 nm in the transition interface between a thick tungsten layer and a carbon layer in the simulation of the experimental $R(\theta)$ curves, obtained with the CuKα_1 radiation, does not appreciably modify the value of the interfacial roughness given by a simple two layer model [40].

4.2 EXAMPLE OF ROUGHNESS EVOLUTION. — The $R(\theta)$ data of figure 5 concerns another (W/C) stack produced on silicon by Barbee. The simulation curve (continuous line) is computed using the same parameter values as before (Tab. II), except for the carbon thickness (5.06 nm) and the roughnesses σ_c (0.375 nm) and σ_w (1.0 nm). If the intensities of the main Bragg peaks are rather well respected, some disagreements are found on the contrasts and the mean intensity of the secondary maxima. It can be noticed, in particular, that the contrast of the experimental secondary fringes gradually decreases until it almost disappears around the fifth main peak.

This can be interpreted by changes in the interfacial roughnesses, as illustrated in figure 6. Two cases have been considered : a regular degradation (continuous curve) or improvment (dashed curve) of

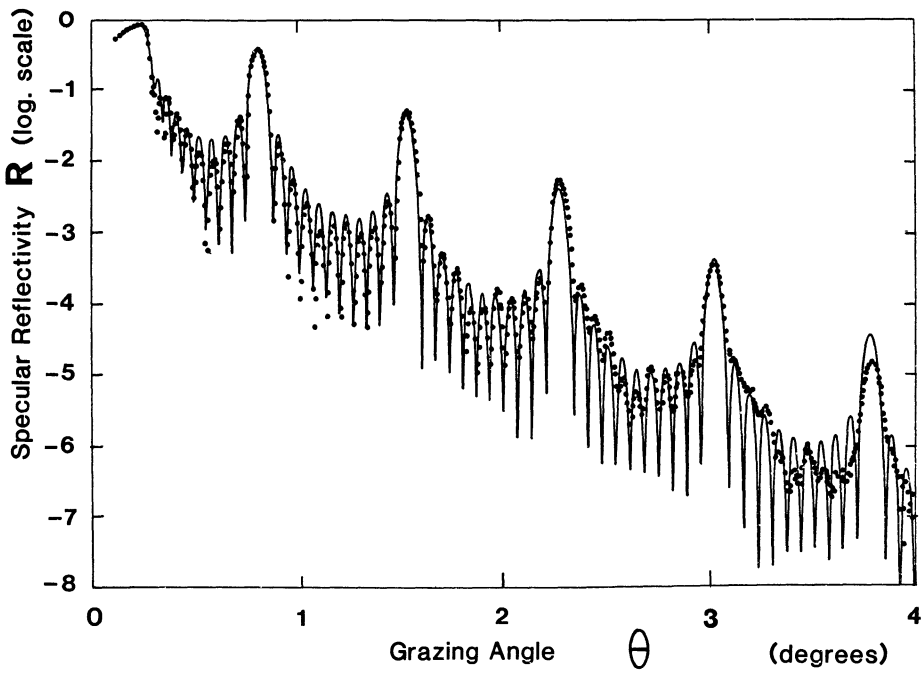

Fig. 5. — Measured (dots) and calculated (solid line) specular reflectivity curves $R(\theta)$ for another W/C multilayer fabricated by T. W. Barbee. The multilayer period is 5.86 nm. The calculation assumes $\sigma_{C/W} = 1$ nm and $\sigma_{W/C} = 0.375$ nm.

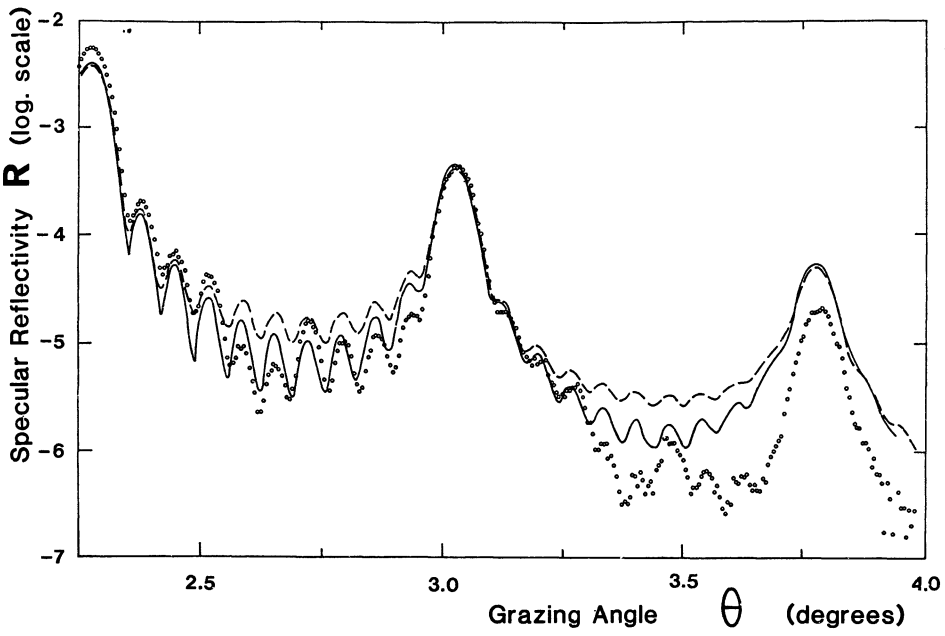

Fig. 6. — Changes on the reflectivity curve when the interfacial roughnesses $\sigma_{W/C}$ increase (solid line) or decrease (dashed line) linearly from the substrate to the top with the same variation (0.025 nm/period). Dots are experimental data.

σ_c, when going from the substrate to the free surface. The absolute roughness variation, from period to period, is the same (0.025 nm) in both cases. On the other hand, the average value is slightly different (0.4 and 0.375 nm respectively) in order to restore the same intensity for the peak of order 5. Not only the contrast of the secondary oscillations, but also their mean intensity between two main Bragg peaks, are modified. It therefore clearly appears that one cannot get rid of the roughness, if one wants to find a direct effect of the thickness deviations, by a simple comparison of the intensities measured at the Bragg half-orders and at the main Bragg peaks [30].

The $R(\theta)$ curves of figure 7 prove that very slight modifications of the evolution of the W/C interfacial roughnesses, in particular the ones on the substrate side, are sufficient to generate modulations on the contrast of the secondary peaks and to increase the intensity difference between the inter-peak background and the main peaks. The σ_c roughness values considered for these two curves are indicated in table III. Notice that the average value $\langle\sigma_c\rangle$ remains the same.

In the case of the continuous curve, the W/C interfacial roughness stays essentially constant over 4 periods, then deteriorates gradually (+ 0.03 nm per period beyond the seventh one). It must be noticed that neither the intensity, nor the half-height width of the main peaks are affected by these roughness changes (roughnesses with the same mean value).

4.3 THICKNESS DEVIATIONS AND ROUGHNESS EVOLUTION. — The $R(\theta)$ data of figure 8 was measured on a stack of 40 tungsten and carbon alternated layers, deposited on a float-glass substrate by Ph. Houdy (L.E.P.). The intensities are expressed in counts/second, without any correction for the background noise (1.6 ct/s in this experiment). The measurements were performed on the second reflectometer at the Institut d'Optique, equipped with a LiF (220) monochromator.

The significant feature in this graph is the dissym-

Table III. — W/C *interfacial roughnesses used for the two reflectivity curves shown in figure 7. Note that the average value is the same in these two distributions.*

C layer	1	3	5	7	9	11	13	15	17	19	21	23
σ (--) nm	0.265	0.288	0.313	0.338	0.363	0.388	0.413	0.438	0.463	0.488	0.513	0.538
σ (—) nm	0.325	0.313	0.313	0.313	0.338	0.359	0.398	0.428	0.458	0.488	0.518	0.548

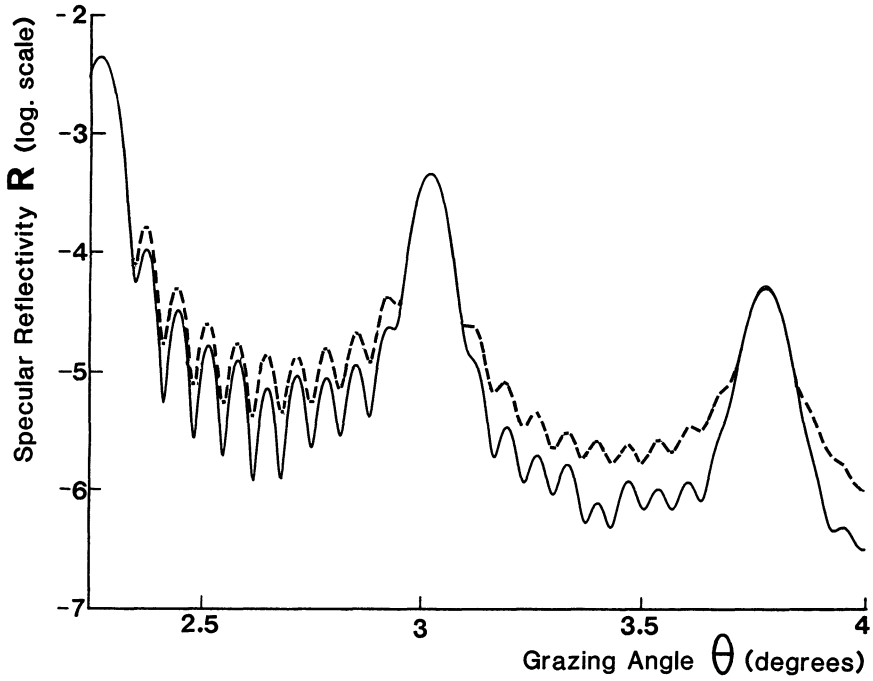

Fig. 7. — Changes on the mean reflectivity between the main Bragg peaks and on the contrasts of the secondary peaks, obtained for two W/C interfacial roughness distributions (see Tab. III), keeping the same mean value (0.4 nm). For the dashed curve, $\sigma_{W/C}$ increase linearly (0.025 nm/period). For the solid curve, $\sigma_{W/C}$ remain, at first constant and then, after the thirteenth C layer, increase linearly (0.03 nm/period) ; the secondary peaks appear more irregular and are in better agreement with the experimental data.

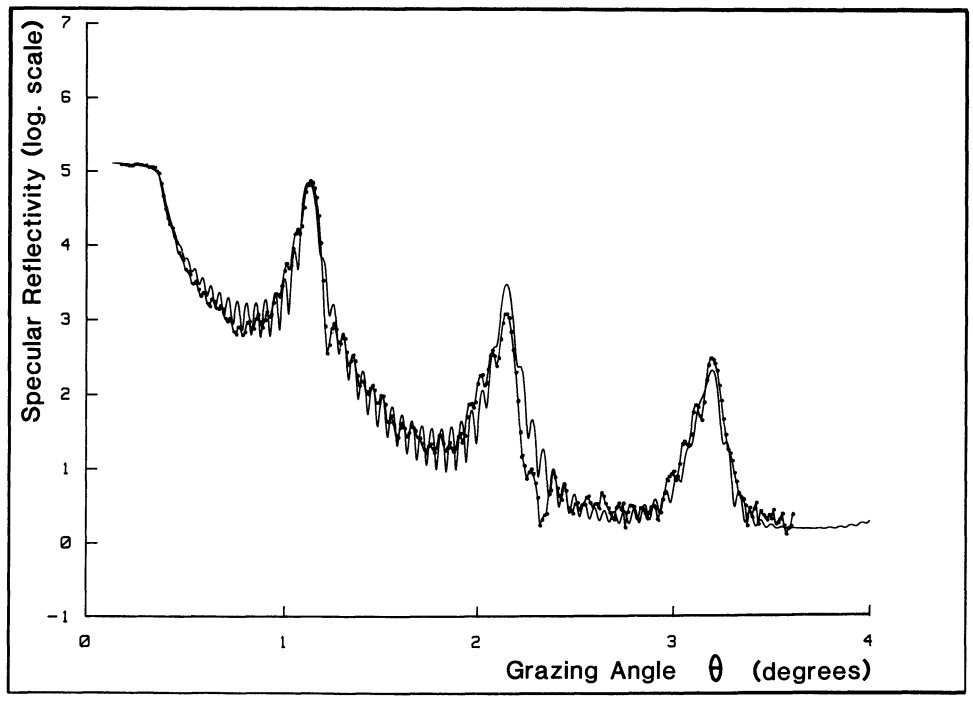

Fig. 8. — Measured (curve with dots) and calculated (solid line) specular reflectivity curves $R(\theta)$ for an (C/W) stack containing 40 layers on a float-glass substrate, fabricated by Ph. Houdy (L.E.P.). The mean multilayer period is 4.18 nm. The calculation assumes a linear decrease of the period (0.01 nm/period) from the substrate to the top, and a similar increase of the W/C interfacial roughness. Note that the reflectivity is measured in arbitrary units (counts/s) and reported without noise correction.

metry of the Bragg peaks. A characteristic widening is observed on the small angle side, together with a climbing of the secondary peaks. This could only be produced by assuming thickness variations of 0.01 nm per period, the average thicknesses $\langle d_c \rangle$ and $\langle d_w \rangle$ being equal to 1.49 and 2.69 nm respectively. If only this dissymetry is considered, the sign of the thickness variation depends on the evolution of the σ_c roughnesses. For example, if σ_c increases, d_c must decrease, and conversely. However, as before in section 4.2, the contrast between the intensity of the inter-peak backgrounds and the main Bragg peaks increases when the σ_c roughness deteriorates from the substrate towards the free surface. This can be explained by a compensation effect between a larger absorption and a smaller roughness. Compared to the waves reflected by the upper layers, the waves which fall upon the lower layers suffer a larger attenuation because of the absorption when passing through the preceding layers, but they are more strongly reflected because of a smaller interfacial roughness. Moreover, these more deeply reflected waves return to the free surface again more easily, due to an improvement of the transmission factor. The amplitudes of the interfering waves become closer to each other, which explains the observed better contrast.

The continuous theoretical curve in figure 8 corresponds to a gradual change of σ_c from 0.2 nm to 0.39 nm at the free surface, the σ_w roughness remaining constant and equal to 0.9 nm. The σ_w values can be varied around this mean value, but the differences induced on $R(\theta)$ are very small and manifest themselves only in the wings of the first Bragg peak, essentially in the contrast of the secondary peaks. The instrumental resolution in this experiment was not sufficient to discriminate between σ_w evolutions in either direction (in order to take into account the slit width, a convolution over 90 seconds of arc was used in the computations). It should be noticed that, under the assumption of the superposition of two random processes for the W layer growth, the σ_w roughness would be related to the intrinsic roughnesses $\sigma_{c,i}$ and $\sigma_{w,i}$ by :

$$\sigma_w^2 = \sigma_{c,i}^2 + \sigma_{w,i}^2 .$$

Provided $\sigma_{w,i}$ is different enough from $\sigma_{c,i}$, the $\sigma_{c,i}$ variation (from 0.2 to 0.4 nm) has only little influence on σ_w.

The experimental $R(\theta)$ data of figure 8 (represented by dots) reveals a few anomalies which can only result from certain irregularities in the evolution of the thicknesses and of the interfacial roughnesses, in particular, on the first deposited layers. The model chosen for the simulation is too regular and is, in fact, only representative of the average tendencies of these evolutions. An analysis performed on companion samples, deposited simultaneously but comprising a smaller number of layers, would probably allow one to remove some ambiguities or deficiencies of this modelization.

5. Conclusion.

The three preceding analyses illustrate the different types of defects encountered in the multilayer structures : a difference of interfacial roughness for the two elementary layers, and an evolution of the roughnesses and of the thicknesses in the stack. These defects are revealed clearly by the grazing X-ray reflection analysis.

If the study of the Bragg maxima intensities is sufficient for a rapid determination of the mean values of the interfacial roughnesses, it is essentially in the analysis of the secondary maxima that the possible presence of a roughness and/or thickness evolution in the stack can be detected. The determination of the direction of these evolutions is not often easy. It requires a very good instrumental resolution and, in particular, an improvement of the signal-to-noise ratio for a correct analysis of the intensities in the vicinity of the Bragg half-orders.

The geometrical characterization, obtained in a non destructive manner by the grazing X-ray reflection analysis, can then be compared to the observation with transverse cuttings of the stacks by high resolution electron microscopy. This last technique allows a more accurate characterization of the structure of the elementary layers and of their interfaces. It must be emphasized that, as far as the evaluation of the interfacial roughnesses is concerned, the two methods appear complementary rather than competitive, the corresponding ranges of spatial frequencies in the roughness spectrum being adjacent rather than common. From such a comparison, it is reasonable to hope for, not only a more critical look at the optical indices as presently established in the X-UV range, but also an improvement of the techniques in preparation of multilayers in order to increase their performances.

Acknowledgments.

The authors are indebted to Dr. T. W. Barbee and Dr. Ph. Houdy for the making of the W/C multilayers and to Dr. M. L. Theye for the translation of the original paper.

References

[1] LOVE, W. P., GEBALLE, T. H., *Phys. Rev. B* **29** (1984) 4961-4968.

[2] SCHULLER, I. K., FALCO, C. M., *Thin Solid Films* **90** (1982) 221-227.

[3] ESAKI, L., *J. Phys. Colloq. France,* **45** (1984) C5, 3-21.

[4] MAJKRZAK, C. F., *Appl. Opt.* **23** (1984) 3524-3527.

[5] SPILLER, E., Handbook on Synchrotron Radiation, Vol. **1**, Ch. 12 « Soft X-Ray Optics and Microscopy » Ed. E. Koch (North Holland) 1983, pp. 1092-1129.

[6] VINOGRADOV, A. V., ZELDOVICH, B. Ya., *Appl. Opt.* **16** (1977) 89-93 ; *Opt. Spectrosc.* **42** (1977) 404-407.

[7] HENKE, B. L., LEE, P., TANAKA, T. J., SHIMABUKURO, R. L. and FUJIKAWA, B. K., *Atomic and Nuclear Data Table* **27** (1982).

[8] GOLUB, L., SPILLER, E., BARTLETT, R. J., HOCKADAY, M. P., KANIA, D. R., TRELA, W. J., and TATCHYN, R., *Appl. Opt.* **23** (1984) 3529-3533.

[9] ARBAOUI, M., BARCHEWITZ, R., SELLA, C. and YOUN, K. B., *S.P.I.E.,* Vol. **652** « Thin Film Technologies » (Innsbruck) 1986, pp. 318-325.

[10] BARBEE, T. W., « Low Energy X-Ray Diagnostics », *AIP Conf. Proc.* **75** (1981) 131-145.

[11] FALCO, C. M., FERNANDEZ, F. E., DHEZ, P., KHANDAR-SHAHABAD, A., NEVOT, L., PARDO, B. and CORNO, J., *S.P.I.E.* Vol. **733** « Soft X-Ray Optics and Technology » Ed. E. Koch, G. Schmall (Berlin) 1986, pp. 343-352.

[12] HOUDY, Ph., BODART, V., HILY, C., RUTERANA, P., NEVOT, L., ARBAOUI, M., ALEYANE, N. and BARCHEWITZ, R., *S.P.I.E.* Vol. **733,** 389-397.

[13] GAPONOV, S. V., GLUSKIN, E. S., GUSEV, S. A., PLANONOV, Yu Ya and SALASHCHENKO, N. N., *Opt. Commun.* **48** (1983) 229-232.

[14] BARBEE, T. W., MROWKA, S. and HETTRICK, M. C., *Appl. Opt.* **24** (1985) 883-886.

[15] SMIRNOV, L. A., SOTNIKOVA, S., ANOKHIN, B. S. and TAIBIN, B. Z., *Opt. Spectrosc.* (USSR) **46** (1979) 329-332.

[16a] CROMER, D. T., LIBERMAN, D., *J. Chem. Phys.* **53** (1970) 1891-1898.

[16b] Intern. Tables for X-ray Crystallography : Vol. **4,** Ch. 2, Ed. J. A. Ibers, W. C. Hamilton (Kynoch Press, Birmingham) 1974.

[17] SMITH, D. Y., *Phys. Rev. A* **35** (1987) 3381-3387.

[18] BORN, M., WOLF, E., *Principles of Optics* (Pergamon Press N.Y) 1965, Third Edition, pp. 51-70.

[19] PARRATT, L. G., *Phys. Rev.* **95** (1954) 359-369.

[20] UNDERWOOD, J. H., BARBEE, T. W., *Appl. Opt.* **20** (1981) 3027-3034.

[21] CROCE, P., NEVOT, L., *J. Appl. Cryst.* **7** (1974) 125-130.

[22] CROCE, P., NEVOT, L., PARDO, B., *Nouv. Rev. Opt. Appl.* **3** (1972) 37-50.

[23] NEVOT, L., CROCE, P., *Rev. Phys. Appl.* **15** (1980) 761-779.

[24] CROCE, P., NEVOT, L., *Rev. Phys. Appl.* **11** (1976) 113-125.

[25] SPILLER, E., ROSENBLUTH, A. E., *S.P.I.E.,* Vol. **563** « Application of Thin Film Multilayered Structure to figured X-ray Optics » Ed. G. F. Marshall (1985), pp. 221-236.

[26] HAELBICH, R. P., SEGMULLER, A., SPILLER, E., *Appl. Phys. Lett.* **34** (1979) 184-186.

[27] POMERANTZ, M., SEGMULLER, A., *Thin Solid Films* **68** (1980) 33-45.

[28] NEVOT, L., Thèse d'Etat, Orsay n° 1954 (1978) ; *Acta Electronica* **24** (1981/1982) 255-265.

[29] BRUIJN, M. P., CHAKRABORTY, P., VAN ESSEN, H., VERHOEVEN, J. and VAN DER WIEL, M. J., *S.P.I.E.,* Vol. **563** (1985) 182-194.

[30] SPILLER, E., ROSENBLUTH, A. E., *S.P.I.E.,* Vol. **563** (1985) 221-236.

[31] SEGMULLER, A., *Thin Solid Films* **18** (1973) 287-295.

[32] BARTELS, W. J., *J. Vac. Sci. Technology* **B 1** (1983) 338-345.

[33] NEVOT, L., PROD'HOMME, L., CROCE, P., Rapport D.G.R.S.T. 78-73055 (1980) Orsay.

[34] HOUDY, Ph., ZIEGLER, E., NEVOT, L., *Thin Solid Films* **141** (1986) 99-109.

[35] CHAUVINEAU, J. P., CORNO, J., NACCACHE, D., NEVOT, L., PARDO, B., VALIERGUE, L., *J. Opt.* (Paris) **15** (1984) 265-269.

[36] CHAUVINEAU, J. P., *Thin Solid Films* **109** (1983) 353-361.

[37] CHAUVINEAU, J. P., CORNO, J., DECANINI, D., NEVOT, L., PARDO, B., VALIERGUE, L., *S.P.I.E.,* Vol. **563** (1985) 245-252.

[38] LEPETRE, Y., RASIGNI, G., RIVOIRA, R., PHILIP, R. and METOIS, J. J., *J. Opt. Soc. Am.* **A 2** (1985) 1356-1362.

[39] PETFORD-LONG, A. K., STEARNS, M. B., CHANG, C. H., NUTT, S. R., STEARNS, D. G., CEGLIO, N. M. and HAWRYLUK, A. M., *J. Appl. Phys.* **61** (1987) 1422-1428.

[40] GASGNIER, M., NEVOT, L., BAILLIF, P., BARDOLLE, J., *Phys. Status Solidi (a)* **79** (1983) 531-542.